Chinese Journal of
POLYMER SCIENCE

RESEARCH ARTICLE

https://doi.org/10.1007/s10118-026-3713-7
Chinese J. Polym. Sci. **2026**, *44*, 2982–2989

Topology-regulated Co-assembly of Single Chain Polymer Nanoparticles and Block Copolymers into Hierarchical Micelle@Vesicle Composite Structures

Bai-Xue Deng[a], Hong-Zhu Lai[b], Li Jiang[b*], Lin Yu[a], Lin Cheng[b], and Dao-Yong Chen[a,b*]

[a] *State Key Laboratory of Molecular Engineering of Polymers, Department of Macromolecular Science, Fudan University, Shanghai 200438, China*
[b] *School of Chemistry and Materials Science, Anhui Normal University, Wuhu 241002, China*

Electronic Supplementary Information

Abstract Polymer co-assembly provides a versatile route to hierarchical nanostructures, yet achieving precise structural control remains a significant challenge. In particular, understanding how topological differences in polymer building blocks influence co-assembly behavior is important for expanding the design of complex polymer materials. In this work, a co-assembly system of amphiphilic block copolymers (BCPs) and single chain polymer nanoparticles (SCPs) was designed to investigate the effect of topological variations. At certain SCP/BCP mass ratios, BCPs and SCPs co-assembled to form a hierarchical composite structure with vesicles growing on the surface of micelles, following a path-dependent stepwise co-assembly mechanism, where SCPs co-assembled with BCP to form core micelles and self-assembled into vesicles from the micelle surface into hierarchical micelle@vesicle (M@V) composite structure. The SCP/BCP mass ratio significantly influences the morphology and size of the M@V composite structure, and the strategy is applicable to copolymer systems with wide range of hydrophobic/hydrophilic volume ratios. This work provides new insights into topology-regulated polymer co-assembly and offers a useful strategy for the design of hierarchical and multifunctional polymer materials.

Keywords Block copolymers; Single chain polymer nanoparticles; Co-Assembly; Micelle@vesicle

Citation: Deng, B. X.; Lai, H. Z.; Jiang, L.; Yu, L.; Cheng, L.; Chen, D. Y. Topology-regulated co-assembly of single chain polymer nanoparticles and block copolymers into hierarchical micelle@vesicle composite structures. *Chinese J. Polym. Sci.* **2026**, *44*, 2982–2989.

INTRODUCTION

Block copolymer (BCP) self-assembly provides an efficient bottom-up approach for constructing well-defined morphologies including micelles, worm-like micelles, and vesicles.[1–3] In selective solvents, the incompatibility between hydrophilic and hydrophobic blocks drives microphase separation, making the assembled morphologies co-regulated by intermolecular interactions, structural parameters, packing, and curvature.[4–6] Due to the well-established correspondence between BCP parameters and assembly morphology, BCP self-assembly systems exhibit excellent predictability and tunability, thus finding widespread applications in delivery systems, nano-reactors, and functional coatings.[7–9] However, despite the high flexibility of BCP self-assembly in morphology control, the accessible structural landscape in single-component BCP systems is ultimately bounded by the finite library of BCP chemistries and limited tunability window of molecular parameters. As the demand for hierarchical structures, complex morphologies, and multifunctional integrated systems continues to increase, single-BCP systems are insufficient for constructing higher-order structures.

Co-assembly has been widely introduced as an important strategy to overcome the limitations in the structural control of single BCP systems. By introducing BCPs and different types of polymer building blocks into the same system, co-assembly can significantly expand the types of assembled morphologies and hierarchical structures.[10–13] In BCP/homopolymer co-assembly systems, the introduction of homopolymer components can effectively adjust the local packing and interfacial composition of the BCP system, resulting in various complex morphologies, such as asymmetric vesicles, helixes, and ring-shaped micelles.[14–16] Additionally, co-assemblies of different BCPs exhibit rich structural diversity. BCP/BCP co-assembly systems have been used to construct asymmetric micelles, composite vesicles, and multilayer structures by rationally designing the block ratios, chain rigidity, and interaction modes.[17–19] Moreover, polymer brushes with special topological structures have also been incorporated into BCP coassembly systems. Because of the dense packing and conformational extension of the brush side chains, they can significantly affect the local packing and interfacial structures

* Corresponding authors, E-mail: jiangli22@ahnu.edu.cn (L.J.)
E-mail: chendy@fudan.edu.cn (D.Y.C.)
Received April 2, 2026; Accepted April 13, 2026; Published online June 9, 2026

during co-assembly, leading to significant impacts on the assembly morphology and hierarchical structure formation.[20] The introduction of polymer building blocks with special topological conformations provides a new structural dimension for regulating BCP coassembly.

Single-chain polymer nanoparticles (SCPs) are nanostructures formed by the intrachain crosslinking of a single polymer chain.[21–23] Compared to linear polymer precursors, SCPs exhibit smaller hydrodynamic diameters, lower chain entanglement, and reduced chain mobility. These structural characteristics enable SCPs to display scale features, conformational stability, and interfacial adaptability and allow SCPs to self-assemble into advanced polymer nanostructures with unique performance.[24–26] By intrachain crosslinking the hydrophilic segment of a BCP, the cross-sectional molecular area is reduced and the packing parameter is remarkably enlarged, making it easier for SCPs to self-assemble into inverse bicontinuous structures. By the aggregation of hydrophobic intrachain crosslinked heads, SCPs self-assembled into ultrasound-responsive superparticles with hydrophilic channels.[27] Janus SCPs, formed by the double crosslinking of two BCP blocks, self-assembled with high exclusivity to form regularly structured macroscopic assemblies.[28] When SCPs and BCPs are expected to coexist in the same self-assembly system, the differences in conformation and interfacial characteristics between the different building blocks may result in entirely new assembly behaviors, thereby providing new possibilities for expanding the structural manifestations of polymer coassemblies.

Herein, we designed a co-assembly system of BCP and SCP to investigate the effect of topological variations on the co-assembly behavior. The coassembly process was performed in an acetone/H_2O mixed solution. At certain SCP/BCP mass ratios, BCPs co-assemble with SCPs to form a hierarchical composite structure, with vesicles growing on the surface of the core micelles (micelle@vesicle, denoted as M@V). Instead of single-step equilibrium co-assembly, we propose a path-dependent stepwise co-assembly mechanism controlled by the SCP ratio. In this stepwise process, SCPs serve as both primary building blocks for co-assembly and units that later self-assemble from the surface to form the M@V composite structures. The SCP/BCP mass ratio significantly influenced the size of the core micelles, the number of vesicles on each micelle, and the overall morphology of the composite structure. Additionally, M@V composite structures were successfully formed in co-assembly systems in which the BCP hydrophobic/hydrophilic volume ratios were varied, demonstrating the applicability of this strategy to a wide range of copolymer systems. This study provides new insights into expanding the structural diversity and functional design of co-assemblies.

EXPERIMENTAL

Materials

Benzyl methacrylate (BZMA, 98%, TCI) and *N,N*-dimethylaminoethyl methacrylate (DMAEMA) were passed through a short basic aluminum oxide column before use to remove the inhibitor. 4,4'-Azobis(4-cyanopentanoic acid) (ACVA) was obtained from TCI and recrystallized from anhydrous ethanol twice before use. 7-(2-Methacryloyloxyethoxy)-4-methylcoumarin (CMA) and RAFT agent 4-cyanopentanoic acid dithiobenzoate (CPADB) were purchased from Sigma-Aldrich. Other solvents (AR) were purchased from Sinopharm Chemical Reagent Co., Ltd. and used as received.

Characterization

^{1}H-NMR spectra of the samples solubilized in $CDCl_3$ were obtained using a Bruker Avance III 400 MHz spectrometer. Gel permeation chromatography was performed using an Agilent 1260 HPLC system equipped with a G1310B pump and *N,N*-dimethylformamide (DMF) with 1.6 g/L LiBr as the eluent at a flow rate of 1.0 mL/min and a temperature of 50 °C. Transmission electron microscopy (TEM) observations were performed using a Hitachi HT7800 transmission electron microscope operating at an accelerating voltage of 100 kV. TEM samples were prepared by depositing a drop of the diluted sample solution onto a carbon-coated copper grid followed by drying under ambient conditions. Field-emission scanning electron microscopy (FE-SEM) images were obtained using a Zeiss Ultra 55 FE-SEM at an accelerating voltage of 2 kV. For the FE-SEM sample preparation, a dilute solution of the sample was deposited onto a silicon wafer, allowed to dry under ambient conditions, and then sputter-coated with gold for 20 s (5 mA). UV-Vis spectra were recorded using a PerkinElmer Lambda 35 spectrophotometer with a conventional quartz cell. Fluorescence imaging was performed using a Zeiss LSM 980 fluorescence microscope, where the samples were observed under bright field, 588 nm laser fluorescence, and an overlay of both fields.

Synthesis of PDBC and PDB

Poly(*N,N*-dimethylaminoethyl methacrylate)-block-poly (benzyl methacrylate-*co*-4-methyl-(7-(methacryloyl) oxy-ethyloxy)-coumarin) (PDMAEMA-*b*-P(BZMA-*co*-CMA), PDBC) and poly(*N,N*-dimethylaminoethyl methacrylate)-block-poly{benzyl methacrylate (PDMAEMA-*b*-PBZMA, PDB) were synthesized following the route outlined in Scheme S1 (in the electronica supplementary information, ESI), as described in our previous work.[29] The characterization data are shown in Figs. S1–S3 (in ESI).

Synthesis of SCP

PDBC (10 mg) was dissolved in 10 mL of acetone and placed in a 20 mL quartz sample bottle, which was stirred until completely dissolved. The solution was then irradiated under a 365 nm UV lamp (36 W) for 4 h to obtain the SCP. The characterization data for the SCP are shown in Fig. S4 (in ESI).

Self-assembly of SCP, PDBC and PDBs

The preparation of self-assemblies was performed as follows: 2.0 mg of SCP, PDBC, PDB1, or PDB2 was dissolved in 1.0 mL of acetone, and then 100 μL of water was added slowly to the solution using a 1.0 mL microsyringe at a rate of 0.2 mL/h under mild stirring at 500 r/min.

Co-assembly of SCP and PDBs

Acetone solutions of SCP and PDB1 were prepared at concentrations of 2 mg/mL. The solutions were mixed at volume ratios of 1/1, 10/1, 20/1, and 50/1, respectively. The mixtures were then stirred thoroughly, and deionized water was added at a rate of 0.2 mL/h using a syringe pump, while maintaining a stirring speed of 500 r/min. Co-assembly of SCP with PDB1-RhB, PDB2, and PDB3 was performed using the same procedure. The self-assembly process and the final assembled structures were

https://doi.org/10.1007/s10118-026-3713-7

characterized using TEM and fluorescence microscopy.

RESULTS AND DISCUSSION

Synthesis and Characterization of PDBC, PDBs and SCP

Amphiphilic block copolymers, PDMAEMA-*b*-P(BZMA-*co*-CMA) (PDBC), designed for the synthesis of SCP and PDMAEMA-*b*-PBZMA (PDB) with varying length ratios of PDMAEMA/PBZMA, were synthesized using reversible addition–fragmentation chain transfer (RAFT) polymerization (Fig. 1a). The degree of polymerization (DP) of the DMAEMA, BZMA, and CMA units was determined by ^{1}H-NMR spectroscopy (PDB1: PDMAEMA$_{54}$-*b*-PBZMA$_{452}$, PDB2: PDMAEMA$_{81}$-*b*-PBZMA$_{374}$, PDB3: PDMAEMA$_{193}$-*b*-PBZMA$_{608}$, Fig. S1 in ESI; PDBC: PDMAEMA$_{81}$-*b*-(PBZMA$_{361}$-*co*-CMA$_{52}$), Fig. S2 in ESI; the subscript indicates the DP of each unit). The molecular weight (M_n) and molecular weight distribution ($Đ$) were further confirmed using DMF size-exclusion chromatography (SEC). As shown in Figs. S3 and S4 (in ESI), the SEC traces for PDBs and PDBC exhibit highly symmetric and narrow peaks, indicating low dispersity ($Đ$<1.2) of the polymers. This low dispersity is essential to ensure the uniformity and high performance of the synthesized polymer structures. SCP was prepared through the photodimerization of coumarin groups in the hydrophobic P(BZMA-*co*-CMA) block under 365 nm UV light irradiation. The elution curve for SCP (Fig. S4 in ESI) showed a shift to longer retention times after the crosslinking reaction, which confirms the occurrence of intrachain crosslinking, resulting in the formation of an amphiphilic SCP with a hydrophobic collapsed domain and a hydrophilic tail.

Co-assembly of SCP and PDB1

To demonstrate the co-assembly behaviors of SCP and PDB, their self-assembly and co-assembly of SCP and PDB were inves-

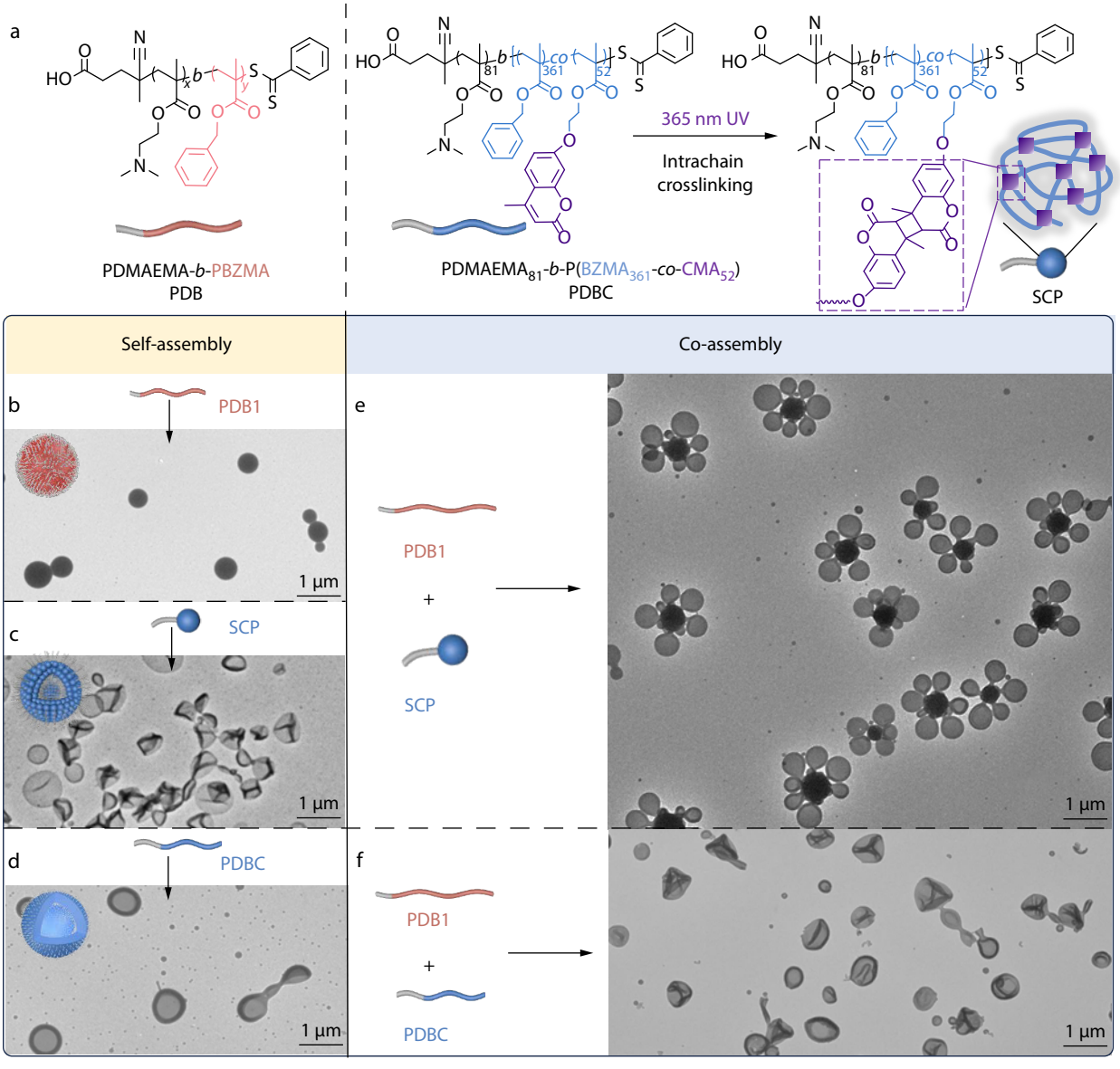

Fig. 1 (a) Chemical structures of PDBs and SCP derived from intrachain crosslinking of PDBC. (b–f) TEM images of respective self-assemblies of PDB1 (b), SCP (c) and PDBC (d), and co-assemblies of SCP/PDB1 (e) and PDBC/PDB1 (f).

https://doi.org/10.1007/s10118-026-3713-7

tigated in parallel. The assembly process was induced by gradually adding water, a selective solvent for PDMAEMA, to the acetone solution of the polymer (with a H_2O/acetone volume ratio of 1/10 and an initial polymer concentration of 2 mg/mL) under stirring. As shown in the TEM images (Figs. 1b and 1c), PDB1 self-assembled into spherical micelles with an average diameter of approximately 620 nm (Fig. 1b), while SCP self-assembled into spherical vesicles of a similar size (Fig. 1c). When SCP and PDB1 were co-assembled at a mass ratio of 20/1, an M@V composite structure was obtained (Fig. 1e). This structure was completely different from those formed by the self-assembly of SCP and PDB1. Therefore, it is hypothesized that this composite structure is formed by the co-assembly of the two polymers with a synergistic interaction between the collapsed SCP and PDB1, promoting the formation of the composite structure. Additionally, when non-cross-linked PDBC (which also forms vesicles upon self-assembly, Fig. 1d) and PDB were co-assembled under the same conditions, uniform spherical vesicles were obtained (Fig. 1f). This suggests that the collapsed hydrophobic domain in the SCP plays a crucial role in inducing the formation of the M@V composite structure.

To clarify the role of the SCP in the co-assembly process, the effect of varying the SCP content on the structure of the co-assembled products was investigated. The TEM image in Fig. 2(a) shows that the assemblies are uniform spherical micelles when the SCP/PDB1 mass ratio is 1/1, the assemblies are uniform spherical micelles. As the SCP/PDB1 mass ratio increased to 10/1, a composite structure consisting of both micelles and vesicles was formed (Fig. 2b), with vesicles clearly visible on the surface of the micelles, resulting in an M@V composite structure. Further statistical analysis showed that at an SCP/PDB1 mass ratio of 10/1, each micelle surface contained an average of 2.1 vesicles. As the SCP/PDB1 mass ratio increased further to 20/1, the structure remained an M@V composite, with the average number of vesicles on the micelle surface increasing to 5.7 (Fig. 2c). When the SCP/PDB1 mass ratio was significantly increased to 50/1, both the M@V composite structures and distinct free vesicles were present in the system (Fig. 2d). The number of vesicles on the micelle surface increased significantly to 14.2. To accommodate more vesicles, the vesicles extend outward from the micelle surface and become necked but still maintain the composite structure with vesicles connected to the micelle surface. This result indicates that the SCP content plays a decisive role in the formation of the composite structure and that by properly controlling the SCP/PDB1 ratio, the structure of the composite assembly can be regulated to some extent. Additionally, statistical analysis of the sizes of the composite assemblies at different SCP/PDB1 mass ratios (Fig. 2e) showed that when the SCP/PDB1 mass ratio was 1/1, the spherical micelles had a size of approximately 213 nm, which was significantly smaller than those formed by PDB self-assembly. When the SCP/PDB1 mass ratio was 10/1, the average size of the spherical micelles in the composite structure was approximately 259 nm. As the SCP/PDB1 mass ratio increased to 20/1 and 50/1, the size of the micelles in the composite structure increased to 470 nm and 776 nm, respectively. The increase in micelle size with decreasing PDB1 content indicates that the micelles are not formed solely by PDB1 self-assembly. Meanwhile, the size of the vesicles in the different composite structures remained approximately constant as the SCP/PDB1 mass ratio increased from 10 to 50, suggesting that the vesicles were likely formed by the self-assembly of SCP, which has a defined packing parameter.

To verify the contribution of SCP and PDB to the structure of the co-assembled product, fluorescence labeling was applied to both SCP and PDB1 (Fig. S5 in ESI) and fluorescence microscopy was used to observe the distribution of each polymer in the assemblies. Fluorescence labeling of SCP and PDB1 had distinct effects on the morphology and structure of the assemblies. When PDB1 was labeled with RhB, the resulting PDB1-RhB did not significantly affect structure of the assembly when co-assembled with SCP, successfully forming the M@V composite structure (Figs. 3a–3d). However, when SCP was fluorescently labeled, the structure of the resulting assembly changed significantly and did not maintain the expected composite structure (Fig. S6 in ESI). Therefore, the dis-

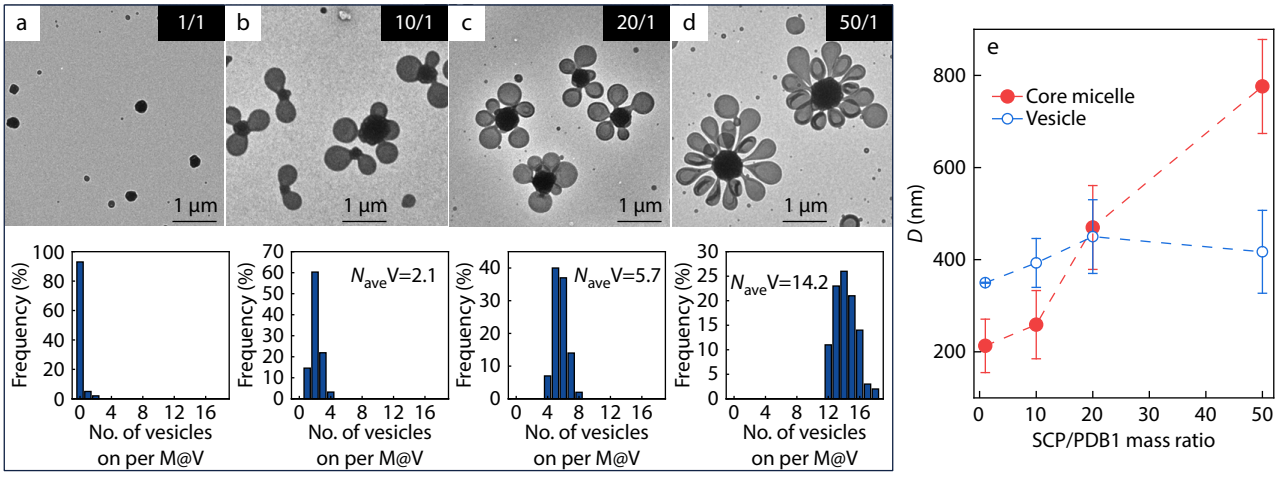

Fig. 2 (a–d) TEM images (top) and histograms illustrating vesicles distribution on micelles (bottom) of polymer nanostructures formed in the co-assembly solution of SCP/PDB1, with SCP/PDB1 mass ratios of (a) 1/1, (b) 10/1, (c) 20/1 and (d) 50/1, respectively. (e) Evolution of diameter of micelles (red squares) and vesicles (black circles) as a function of SCP/PDB1 mass ratio. Error bars indicate standard deviation.

https://doi.org/10.1007/s10118-026-3713-7

tribution of PDB1-RhB in the composite assembly, the composition of different structures in the composite co-assembly was further investigated. Fluorescence microscopy images of the assemblies at different SCP/PDB1 ratios (Fig. 3) showed that PDB1-RhB was only present in the micelle region, and no PDB1-RhB signal was observed in the vesicle structures growing outside the micelles, indicating that the external vesicle structures were completely formed by self-assembly of SCP alone. Although SCP was not directly observed in the micelle structures, the increase in micelle size with decreasing PDB1 content and increasing SCP content (Fig. 2e) suggests that the micelles in the composite structure were co-assembled by SCP and PDB1.

Mechanism of M@V Formation

Based on the composition of the M@V composite structure, its formation is suggested to occur in two steps (Fig. 4a): (1) driven by hydrophobic interactions, the hydrophobic block of PDB and the hydrophobic domain of SCP aggregate to form co-assembled micelles. Owing to differences in length and conformation between the hydrophobic parts of SCP and PDB, and because the crosslinked hydrophobic domain of SCP cannot adjust its conformation through stretching or contraction to adapt to the co-assembly with PDB, the co-assembled structure struggles to achieve effective minimization of local energy. The hydrophilic chain of a single SCP requires a relatively large hydrophobic region for stabilization (Fig. 4b). When these hydrophobic regions are not fully stabilized, the exposed hydrophobic parts act as seeds for further assembly at the micelle surface, thereby providing active sites for vesicle growth. (2) With a further hydrophobic driving force, SCPs in solution that do not participate in micelle formation preferentially accumulate at high-energy hydrophobic interfaces. Based on the structural parameters of SCP, they spontaneously assemble into vesicles on the micelle surface. This process is analogous to the crystallization-driven self-assembly. As the SCP/PDB mass ratio increased, the SCP content on the surface of the coassembled micelles increased, leading to a decrease in the curvature toward the low-curvature state characteristic of the SCP self-assembly (Fig. 4b). Simultaneously, the micelle size increases, providing more active sites for vesicle growth. Furthermore, as the amount of SCP not involved in the co-assembly increases, SCP molecules are more likely to aggregate and grow at these active sites on the micelle surface, further promoting vesicle formation.

To further validate the proposed mechanism of composite structure growth, a reference experiment was conducted in which solutions of SCP and PDB1, self-assembled under identical conditions, were mixed at an SCP/PDB1 mass ratio of 10/1. The TEM images revealed that the mixed solution con-

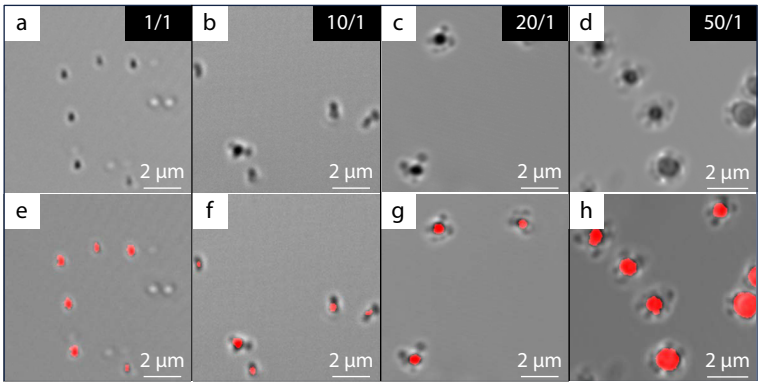

Fig. 3 Bright-field microscopy images (a–d) and the corresponding fluorescence-overlaid images (e–h) of polymer nanostructures formed in the co-assembly systems of SCP/PDB1, with mass ratios of SCP/PDB1 (a, e) 1/1, (b, f) 10/1, (c, g) 20/1 and (d, h) 50/1, respectively.

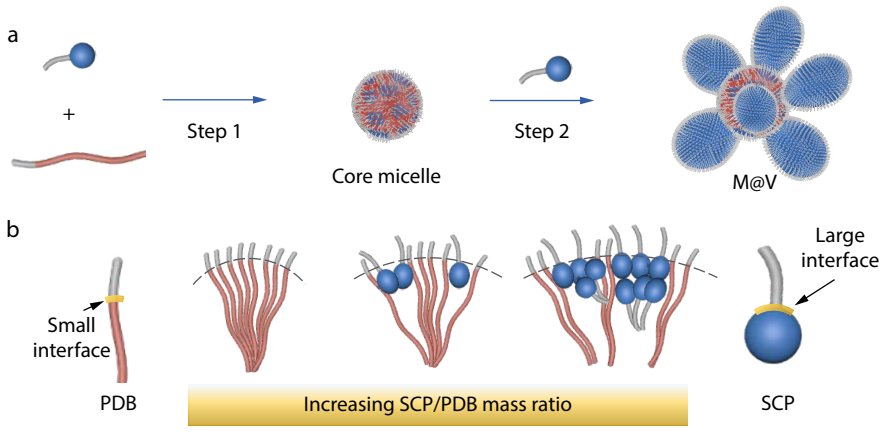

Fig. 4 Schematic illustration of the proposed mechanism for the stepwise co-assembly of SCP and PDBs. (a) Co-assembly of SCP and PDB into core micelle and SCP vesicles assembled from surface of the core micelles; (b) Distribution and surface curve of SCP and PDB on the surface the core micelles with increased mass ratio of SCP.

https://doi.org/10.1007/s10118-026-3713-7

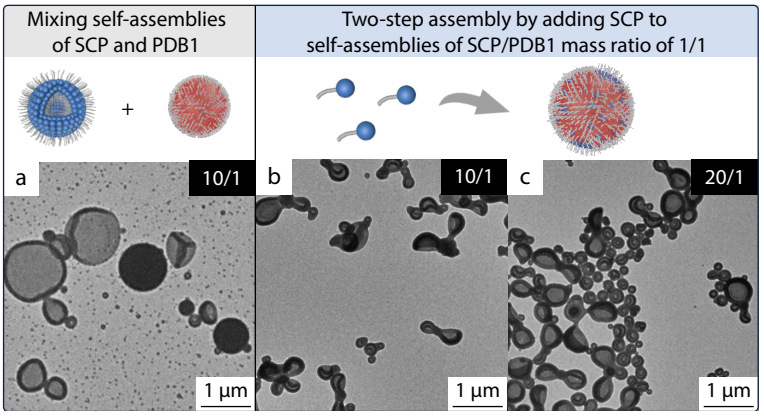

Fig. 5 TEM images of the assemblies obtained from: (a) mixing the pre-assembled SCP and PDB1 solutions with SCP/PDB1 mass ratio of 10/1; (b, c) further adding SCP to the pre-formed assemblies with an initial SCP/PDB1 mass ratio of 1/1, followed by continued water addition to induce further assembly, where the final SCP/PDB1 mass ratios were 10/1 for (b) and 20/1 for (c).

tained only independent spherical vesicles and micelles, with no observed composite structure formation (Fig. 5a). This indicates that the self-assembled structures of SCP and PDB1 were stable, and that the composite structure was not formed through direct interactions between the assemblies. To further confirm the proposed two-step assembly mechanism, independent stepwise reference assembly processes were conducted. The co-assembled micelles of SCP/PDB1 were prepared at a 1/1 mass ratio. Subsequently, SCP dissolved in acetone was added to achieve an SCP/PDB1 mass ratio of 10/1, followed by the addition of water to induce further assembly. TEM images showed that the stepwise assembly resulted in the formation of an M@V composite structure with an average vesicle number of approximately two (Fig. 5b). When the SCP/PDB1 mass ratio was increased to 20/1, the composite structure remained unchanged and no additional vesicles were formed on the micelle surface (Fig. 5c). This is likely due to the limited amount of SCP in the pre-formed micelles and the reduced number of active sites on the micelle surface, making it difficult for excess SCP to grow further and form more vesicles. As the SCP/PDB1 mass ratio increased, the growth of the composite structure became limited by the number of active sites on the micelle surface, indicating that the SCP ratio is crucial for determining the formation of the composite structure and growth of vesicles.

Generality of M@V Formation

To further verify whether the composite structure can form in a broader range of polymer systems, co-assembly of SCP and PDB2 with a hydrophobic/hydrophilic volume ratio similar to that of PDBC and PDB3 with a smaller hydrophobic/hydrophilic volume ratio was conducted (Fig. 6). The TEM images show that both PDB2 and PDB3 co-assembled with SCP to form M@V composite structures (Figs. S7 and S8 in ESI). Because PDB2 self-assembled into spherical vesicles similar to those formed by SCP (Fig. S9 in ESI), suggesting that the micelles in the resulting M@V composite structure were formed by co-assembly of SCP and PDB2. Additionally, at the SCP/PDB2 mass ratio of 50/1, the micelles in the M@V composite structure formed with PDB2 were larger, but the number of vesicles was lower. This could be because PDB2, with a structural parameter

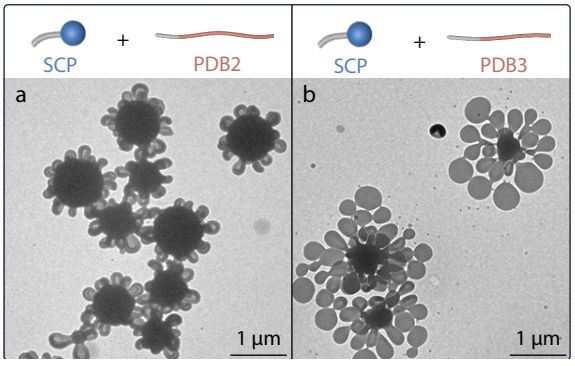

Fig. 6 TEM images of the composite assemblies formed by SCP and PDBs with different structural parameters at an SCP/PDB mass ratio of 50/1: (a) SCP/PDB2, (b) SCP/PDB3.

similar to SCP, more readily forms high-curvature composite micelles, while the complementary interaction between the two components effectively reduces the exposure of hydrophobic regions, leading to fewer active sites on the micelle surface, thus limiting the number of vesicles. This also suggests the effects of the structural parameters of the PDB on the composite structure.

CONCLUSIONS

In conclusion, a co-assembly system of BCPs and SCPs was successfully constructed, revealing the significant impact of topological variations on assembly behavior. At specific SCP/BCP mass ratios, BCPs and SCPs co-assembled to form hierarchical composite structures with vesicles growing on the surface of the core micelles. A path-dependent stepwise co-assembly mechanism controlled by the SCP ratio was proposed, distinguishing it from single-step equilibrium co-assembly. The SCP/BCP mass ratios regulate the size and morphology of the composite structures, and this strategy is applicable to copolymer systems with varying hydrophobic/hydrophilic volume ratios. These findings expand the structural diversity and functional design of polymer co-assembly systems, providing new insights into the design of tunable polymer nanostructures with complex hierarchical features for advanced applications.

https://doi.org/10.1007/s10118-026-3713-7

Conflict of Interests

The authors declare no interest conflict.

Electronic Supplementary Information

Electronic supplementary information (ESI) is available free of charge in the online version of this article at http://doi.org/10.1007/s10118-026-3713-7.

Data Availability Statement

Data supporting the findings of this study are available from the corresponding author upon reasonable request.

ACKNOWLEDGMENTS

This study was financially supported by the National Natural Science Foundation of China (Nos. 52293473 and 22301022).

REFERENCES

1 Zhang, L.; Eisenberg, A. Multiple morphologies of "crew-cut" aggregates of polystyrene-*b*-poly(acrylic acid) block copolymers. *Science* **1995**, *268*, 1728–1731.
2 Discher, B. M.; Won, Y. Y.; Ege, D. S.; Lee, J. C. M.; Bates, F. S.; Discher, D. E.; Hammer, D. A. Polymersomes: tough vesicles made from diblock copolymers. *Science* **1999**, *284*, 1143–1146.
3 Mai, Y.; Eisenberg, A. Self-assembly of block copolymers. *Chem. Soc. Rev.* **2012**, *41*, 5969–5985.
4 Wong, C. K.; Qiang, X.; Müller, A. H. E.; Gröschel, A. H. Self-assembly of block copolymers into internally ordered microparticles. *Prog. Polym. Sci.* **2020**, *102*, 101211.
5 Feng, H.; Lu, X.; Wang, W.; Kang, N. G.; Mays, J. W. Block copolymers: synthesis, self-assembly, and applications. *Polymers* **2017**, *9*, 494.
6 Deng, Z.; Liu, S. Emerging trends in solution self-assembly of block copolymers. *Polymer* **2020**, *207*, 122914.
7 Kuperkar, K.; Patel, D.; Atanase, L. I.; Bahadur, P. Amphiphilic block copolymers: their structures, and self-assembly to polymeric micelles and polymersomes as drug delivery vehicles. *Polymers* **2022**, *14*, 4702.
8 Cabral, H.; Miyata, K.; Osada, K.; Kataoka, K. Block copolymer micelles in nanomedicine applications. *Chem. Rev.* **2018**, *118*, 6844–6892.
9 Ikkala, O.; ten Brinke, G. Functional materials based on self-assembly of polymeric supramolecules. *Science* **2002**, *295*, 2407–2409.
10 Fan, Y.; Ma, J.; Li, Y.; Huang, X.; Feng, S.; Chen, D. Co-assembly of synthetic particles with heterogenous components. *Chem. Mater.* **2024**, *36*, 4011–4033.
11 Ianiro, A.; Chi, M.; Hendrix, M. M. R. M.; Koç, A. V.; Eren, E. D.; Sztucki, M.; Petukhov, A. V.; de With, G.; Esteves, A. C. C.; Tuinier, R. Block copolymer hierarchical structures from the interplay of multiple assembly pathways. *Polym. Chem.* **2020**, *11*, 2305–2311.
12 Doerk, G. S.; Yager, K. G. Diversifying self-assembled phases in block copolymer thin films via blending. *Phys. Rev. Mater.* **2023**, *7*, 120301.
13 Jiang, Z.; Liu, H.; He, H.; Ribbe, A. E.; Thayumanavan, S. Blended assemblies of amphiphilic random and block copolymers for tunable encapsulation and release of hydrophobic guest molecules. *Macromolecules* **2020**, *53*, 2713–2723.
14 Xie, W.; Zhang, T.; Guo, R.; Shi, Y.; Saven, J. G.; Pochan, D. J. Electrostatic coassembly of coiled-coil peptide bundlemers with complementary charges into porous 2D lattices. *J. Am. Chem. Soc.* **2025**, *147*, 47138–47149.
15 Kim, M.; Zhang, M.; Zhu, Y. L.; Yan, Y.; Pu, X.; Choi, W.; Chung, S.; Cho, K.; Kim, J.; Tsukruk, V.; Yang, Z.; Kotov, N. A.; Lu, Z.-Y.; Kim, D. H.; Lin, Z. Hierarchical chiral supramolecular assemblies with strong and invertible chiroptical properties. *Science* **2025**, *389*, eadu0296.
16 Tung, S. H.; Kalarickal, N. C.; Mays, J. W.; Xu, T. Hierarchical assemblies of block-copolymer-based supramolecules in thin films. *Macromolecules* **2008**, *41*, 6453–6462.
17 Chen, Q.; Tian, K.; Zhu, R.; Ding, M.; Xu, Z. Self-assembly of amphiphilic comb-like copolymers into micelles and vesicles in solution. *Polymers* **2025**, *17*, 1870.
18 Ji, M. J.; Li, M.; Chen, C. F. Circularly polarized luminescence of macromolecular co-assembly systems. *Chem. Sci.* **2025**, *16*,

Graphical Abstract

Topology-regulated Co-assembly of Single Chain Polymer Nanoparticles and Block Copolymers into Hierarchical Micelle@Vesicle Composite Structures

Bai-Xue Deng, Hong-Zhu Lai, Li Jiang, Lin Yu, Lin Cheng, and Dao-Yong Chen

Fudan University; Anhui Normal University

Topology-regulated co-assembly of single-chain polymer nanoparticles and block copolymers proceeds through a stepwise pathway, forming hierarchical micelle@vesicle composite structures and offering a new strategy for constructing complex polymer assemblies.

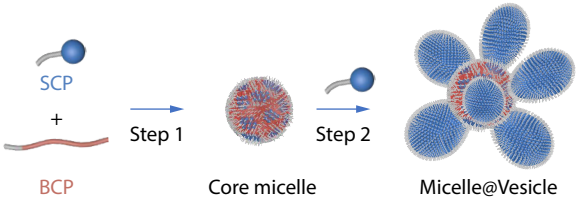

Chinese J. Polym. Sci. 2026, 44, 2982–2989 *https://doi.org/10.1007/s10118-026-3713-7*

12277–12292.
19 Tsaur, L.; Nieves-Rosado, L. A.; Prajwal, B. P.; Zhang, Q.; Li, Y. M.; Escobedo, F. A.; Wiesner, U. B. Film surface assemblies from chemically distinct block copolymer micelles. *Nat. Commun.* **2025**, *16*, 9993.
20 Hou, W.; Zhang, Z.; Shi, Y.; Chen, Y. Co-assembly of diblock copolymers and molecular bottlebrushes. *Macromolecules* **2022**, *55*, 6364–6371.
21 Shao, Y.; Wang, Y. L.; Tang, Z.; Wen, Z.; Chang, C.; Wang, C.; Sun, D.; Ye, Y.; Qiu, D.; Ke, Y.; Liu, F.; Yang, Z. Scalable synthesis of photoluminescent single-chain nanoparticles by electrostatic-mediated intramolecular crosslinking. *Angew. Chem. Int. Ed.* **2022**, *134*, e202205183.
22 Arena, D.; Verde-Sesto, E.; Rivilla, I.; Pomposo, J. A. Artificial photosynthases: single-chain nanoparticles with manifold visible-light photocatalytic activity for challenging "in water" organic reactions. *J. Am. Chem. Soc.* **2024**, *146*, 14397–14403.
23 Chen, R.; Berda, E. B. 100th Anniversary of macromolecular science viewpoint: re-examining single-chain nanoparticles. *ACS Macro Lett*. **2020,** *9*, 1836–1843.
24 Li, W.; Thanneeru, S.; Kanyo, I.; Liu, B.; He, J. Amphiphilic hybrid nano building blocks with surfactant-mimicking structures. *ACS Macro Lett.* **2015**, *4*, 736–740.
25 Wen, J.; Yuan, L.; Yang, Y.; Liu, L.; Zhao, H. Self-assembly of monotethered single-chain nanoparticle shape amphiphiles. *ACS Macro Lett.* **2013**, *2*, 100–106.
26 Wen, W.; Guan, S.; Yang, Z.; Chen, A. Inverse bicontinuous structure by polymerization-induced self-assembly against single-chain nanoparticles. *ACS Macro Lett.* **2021**, *10*, 603–608.
27 Zhou, F.; Xie, M.; Chen, D. Structure and ultrasonic sensitivity of the superparticles formed by self-assembly of single chain Janus nanoparticles. *Macromolecules* **2013**, *47*, 365–372.
28 Jiang, L.; Xie, M.; Dou, J.; Li, H.; Huang, X.; Chen, D. Efficient fabrication of pure, single-chain Janus particles through their exclusive self-assembly in mixtures with their analogues. *ACS Macro Lett.* **2018**, *7*, 1278–1282.
29 Dou, J.; Yang, R.; Du, K.; Jiang, L.; Huang, X.; Chen, D. A General method to greatly enhance ultrasound-responsiveness for common polymeric assemblies. *Polym. Chem.* **2020**, *11*, 3296–3304.

https://doi.org/10.1007/s10118-026-3713-7